A Theoretical Study of the Sea and Land Breezes of Circular Islands

J. NEUMANN[1] AND Y. MAHRER

Dept. of Atmospheric Sciences, The Hebrew University of Jerusalem, Israel

(Manuscript received 19 April 1973, in revised form 10 May 1974)

ABSTRACT

The axisymmetric sea and land breezes of circular islands are studied. First we show, from the equation of turbulent energy, that the marked horizontal convergence of the sea breeze intensifies the turbulence in the flow and that this conclusion affects the equations that model the turbulence. Next, the equations of motion are integrated numerically for two circular islands: a "large" island of radius 51.25 km and a "small" island of radius 26.25 km. The horizontal grid is 2.5 km and the vertical 100 m beginning from the top of a postulated constant-flux layer 25 m thick.

LARGE ISLAND. The sea-breeze front (SBF) is much better developed than in the case of a straight coast. In the first hours of the afternoon the low-level winds ahead of the front are nearly opposite in direction to those of the sea breeze behind the front. There is a strong horizontal convergence in advance of, and divergence behind, the front up to an altitude of 400–500 m; the reverse distribution is the case aloft, where the winds ahead of the surface position of the front depart from the picture of a countercirculation and blow in the same direction as the sea breeze near the surface. The maximum computed upward velocity occurs about the front and reaches 50 cm sec^{-1}. The most surprising feature is the formation in the afternoon of an "eye" of downward velocities around the island center ahead of the front. By late afternoon, however, the island center becomes the center of upward motion. All the above events are connected with an instability developing about the SBF, including the evolution of a pressure low about the surface position of the front. This low deepens as the front moves inland. The land breezes are horizontally divergent with the largest speeds found over the sea.

SMALL ISLAND. The SBF reaches the center about 1300 local time so that little development can take place along the front. However, the upward velocities reach 150 cm sec^{-1} over the center.

In conclusion, it is pointed out that the most interesting features of the sea breeze occur well inland, whereas those of the land breeze occur well offshore.

1. Introduction

In two recent papers (Neumann and Mahrer, 1971, 1973) we have studied the dynamics of the sea- and land-breeze circulation (SLBC) for a *straight* coastline. Our model has adopted several features of Estoque's (1961, 1962) model but it differs from his in some important respects. For instance, in our basic equations we retain the equation of continuity in its "original" form while Estoque uses its vertical derivative. Also, we use the full equation for the vertical component (w) of motion which is required by the numerical procedure adopted by us for integrating the equations. Order-of-magnitude estimates indicate, however, that a retention of the full w equation is necessary for dynamical reasons whenever one wishes to study the motions near the sea-breeze front (SBF) in detail[2] where observations indicate the development of upward velocities of 2 m sec^{-1} and more (see Section 6 where relevant observations are quoted). Finally, some of the important boundary conditions of our model differ from those of Estoque's.

The purpose of the present paper is to study the dynamics of the SLBC for *circular* islands. Since we exclude large-scale pressure gradients and, hence, the motions attendant on such gradients, and since the radii of the islands involved are not so large as to require taking account of the variation of the Coriolis parameter with latitude, our model possesses axial symmetry: the model is two-dimensional in space.

2. Turbulence over islands (circular)

In our first experiments we used the expression for the eddy viscosity (and conductivity) for conditions of forced convection,[3] $K=[k_0(z+z_0)(1+\alpha \mathrm{Ri})]^2(\partial U/\partial z)$, with the same value of the nondimensional constant $\alpha=-0.3$ as adopted in our study for a straight shoreline (Neumann and Mahrer, 1971, p. 533). With this α value the sea breeze continued into the night and we were not able to start the land breeze, although in the model the island surface went on cooling rela-

[1] On leave 1972–73 at the Department of the Geophysical Sciences, The University of Chicago.

[2] By comparing a hydrostatic model with an anelastic two-dimensional, dry, shallow primitive equation model for various horizontal grid sizes, heat inputs and static stabilities, Pielke (1972) finds that at horizontal-to-vertical grid ratios $\leqslant 3$, the hydrostatic model becomes unsatisfactory. This is particularly so for unstable air. Still less satisfactory would the hydrostatic approximation be for a "moist" circulation.

[3] A list of symbols is given in Appendix A.

tive to the sea in accordance with boundary conditions (19) and (20) below.

It will be noted that $(-1/\alpha)$ is a sort of "critical" Richardson number (Ri). Actually, the above expression for K is limited to Ri $\leq(-1/\alpha)$ [see Section 3b], but it is clear that when the value of Ri is close to that of $(-1/\alpha)$, turbulence in the model is at a very low level. With $\alpha=-0.3$, this state of affairs is attained early in the evening and, as a result, there is no mechanism in the model to conduct away the heat carried up to heights of a few hundred meters earlier in the day by the turbulence and the strong vertical motions evolving in the vicinity of the SBF after about midday; winds at these heights continued to blow toward the sea until late hours, forcing the surface flow to continue to be directed from sea to land, that is, the low-level "sea breezes" were maintained. When we reduced the numerical value of α to -0.03, the land breezes set in "in order." A physical interpretation of this situation is described in the next paragraphs.

a. Increased production of turbulent energy due to horizontal shear

The usual assumption made in micrometeorology is that all the shear of the mean horizontal wind is along the vertical, and none is in the horizontal plane. But along a convex coast (convex toward the sea) the sea breezes are convergent (Byers and Rodebush, 1948; Neumann, 1951a, b), that is, they have a shear in the horizontal plane. Theoretical studies such as those by McPherson (1970) for a polygonal coast, and even those of Neumann and Mahrer (1971, 1973) for the vicinity of the SBF developing in the case of a straight shoreline, display a marked horizontal shear of the sea breezes.

Now the equation for the turbulent kinetic energy (TKE) (Lumley and Panofsky, 1964, pp. 67–68) includes terms representing the production of TKE by the interaction of the Reynolds stresses with the shears in the mean flow of the form

$$-\overline{u_i'u_j'}\frac{\partial\bar{u}_i}{\partial x_j}. \tag{1}$$

In meteorology the most commonly considered term is, of course, symbolized by $i=1$ and $j=3$, or $-\overline{u'w'}(\partial\bar{u}/\partial z)$. But if the horizontal shear is strong, then such terms as $-\overline{u'^2}(\partial\bar{u}/\partial x)$ and also, possibly, $-\overline{v'^2}(\partial\bar{v}/\partial y)$ might become important. A recent study (Neumann, 1973) finds that in the neighborhood of the SBF of a straight coastline, the term $-\overline{u'^2}(\partial\bar{u}/\partial x)$ is at least about one-quarter of the term $-\overline{u'w'}(\partial\bar{u}/\partial z)$, that is, the former is no longer negligible. In the case of a not-too-large island, the horizontal convergence, or the horizontal shear, is even greater and we may expect that the associated TKE production rate is comparatively high. From the equation of continuity for an axisymmetric flow [(11) below], we have

$$\frac{\partial u}{\partial r}+\frac{u}{r}=-\frac{\partial w}{\partial z}, \tag{2}$$

where u and w without overbars can be regarded as representing mean flow components. Let us consider the situation close behind the front, that is, on its seaward side. One anticipates the sea breezes of a circular island to be markedly convergent in the horizontal, that is, we expect $\partial u/\partial r$ to be strongly negative (see Figs. 4 and 5 for the early afternoon hours). Since $u<0$ for sea breezes, both terms on the left side of (2) are negative. Moreover, the usual order-of-magnitude estimates would postulate both terms to be of the same magnitude, which means that $\partial w/\partial z$ [and $(\partial w/\partial z)>0$ just in the rear of the front] is large. Suppose now we fix an island radius, choose it as the x axis of a Cartesian coordinate system, and compare flow conditions along that radius with those of the SLBC of a straight coast. In the latter case the x axis will be taken perpendicular to the coast. Because of the notably increased horizontal convergence of the island case, $|\partial u/\partial x|$ along the fixed radius will be notably greater than for the straight coast where in both instances we examine the situation close behind the front. We therefore expect that the production of TKE involving the horizontal shear $(\partial u/\partial x)$ in (1) will be enhanced compared with the straight coast; that is, we anticipate the TKE per unit mass in the island circulation to be appreciably larger than in the straight-coast case. One may add that the above considerations are borne out by our numerical calculations.

Since turbulence is a three-dimensional motion, any increase in the level of turbulence through the enhanced production of TKE by horizontal shear will affect the turbulence along the vertical as well so that turbulence will persist up to a higher Richardson number. For a more quantitative discussion of this point see Neumann (1973). A high Richardson number does not necessarily mean a very low level of turbulence.

Evidence that turbulence along the vertical is intensified is offered by a consideration of the rate of change with height of the vertical flux of horizontal momentum. If we (i) multiply (2) by u, (ii) introduce the identity $u(\partial w/\partial z)=[\partial(uw)/\partial z]-w(\partial u/\partial z)$, (iii) write [as usual in turbulence work] $u=\bar{u}+u'$, (iv) replace r by x in the first term on the right side of (2a), and then (v) average over time (overbar), we find that

$$\frac{\partial(-\bar{u}\bar{w})}{\partial z}+\frac{\partial(-\overline{u'w'})}{\partial z}=\left[\frac{1}{2}\frac{\partial(\bar{u}^2+\overline{u'^2})}{\partial x}-\bar{w}\frac{\partial\bar{u}}{\partial z}-\overline{w'\frac{\partial u'}{\partial z}}\right]+\frac{\bar{u}^2}{r}+\frac{\overline{u'^2}}{r}, \tag{2a}$$

where the sum in brackets on the right side is common to both the straight coast and the island flows. The remaining two terms are positive at all times, and are important near the island center (small r). Assuming for the air layer near the surface that the first term on the left can be ignored relative to the second (and this can be justified by order-of-magnitude analysis), and that near the surface the vertical flux tends to decrease with altitude, we can infer that the presence of the term $[(\bar{u}^2+\overline{u'^2})/r]$ on the right has the effect of slowing down the usual decrease of the vertical turbulent flux with height. This means that the rate of falloff of turbulent energy production with height is less rapid in the island case (near the center) than in the case of a straight coast.

The inference from the foregoing discussion is that in the case of the island flow we may expect an intensified turbulence during the hours of sea breeze.[4] Consequently, the "critical" Richardson number $(-1/\alpha)$ of that flow should be higher, or $-\alpha$ smaller, than is the case for the straight coastline. In our present experiments we have adopted a value $\alpha=-0.03$ and note that the same value was used by McPherson (1970, p. 772) in his study of the sea breeze for a polygonal shoreline involving important horizontal shears.

b. *Horizontal diffusion*

The enhanced intensity of turbulence inferred above is corroborated by a reference to the expression representing diffusion in an axially symmetric flow with a constant horizontal diffusion coefficient K_H. This expression is [see, e.g., Rosenthal, 1970, Eq. (3)]

$$\frac{K_H}{r^2}\frac{\partial}{\partial r}\left[r^3\frac{\partial}{\partial r}\left(\frac{u}{r}\right)\right]=K_H\left[\left(\frac{\partial^2 u}{\partial r^2}\right)+\frac{1}{r}\frac{\partial u}{\partial r}-\frac{u}{r^2}\right]. \quad (3)$$

On the right side the term in parentheses is common to the straight coast and the circular island flows, whereas the remaining two terms are peculiar to the latter. Just ahead of the SBF $(\partial^2 u/\partial r^2)$ is negative[5] as is $(\partial u/\partial r)$; and, for the large island, between about 1330 and 1600 local time, $u>0$. Thus, in the area and the period stated, horizontal diffusion is much stronger than is the case for a straight shoreline.

c. *The form of K in conditions of extreme stability*

It was noted in the opening sentences of this section that the expression for K in conditions of forced convection is considered valid up to Richardson numbers $\mathrm{Ri}<(-1/\alpha)$. In order to let the land breezes carry on in an acceptable pattern during the remainder of the night at still higher Richardson numbers, we have conducted some trials concerning the form of K. Setting $-\alpha$ at a value smaller than 0.03 has not led to success. Several investigators [e.g., Obukhov, 1971; Ellison, 1957, p. 460; and see discussions in Monin and Yaglom (1971) on pp. 448 and 483] have proposed that at extreme stability K is a constant independent of height, that is, the wind profile is linear in the constant flux layer. Our experiments with $K=2\times10^4$ cm^2 sec^{-1} at $\mathrm{Ri}\geqslant 33$ seemed to assure a reasonable continuation of the land-breeze circulation.

Some comments are called for on the high Richardson numbers figuring in this study for the evening-to-morning phase of the circulation. First, when the Richardson number is computed for the lower atmosphere, based on the differences of potential temperature and wind between the "tops" and "bottoms" of vertical grid intervals of finite thickness, the resulting Richardson number is larger than the parallel number for a thinner layer and still larger than the point values of this number within the layer. Second, we have discussed in Section 2a the effect of important horizontal convergences in the mean flow upon the Richardson number.

3. The model

a. *General remarks*

As in our previous studies, we assume that initially, $t<0$, the atmosphere is at rest in hydrostatic equilibrium, which implies that temperature and pressure are uniform along horizontal surfaces (earth curvature is neglected). At time $t=0$, which we take to correspond with 0800 local time, we impress on the island surface a diurnal temperature wave; the sea surface temperature is taken to remain constant. Due to heating of the land, motion sets in in the atmosphere, turbulence develops, and the temperature and pressure distributions change. We assume that, near the surface, turbulence is responsible for the vertical transfers of horizontal momentum and sensible heat; water vapor transport is not mentioned because the circulation is taken to be "dry".[6] The possibility of a significant horizontal diffusion of momentum and heat will be discussed briefly in Section 4.

Following Estoque (1961, 1962) we divide the atmosphere affected by the SLBC into two layers: (i) a relatively thin surface layer in which the vertical fluxes of momentum and heat are constant with height, and, surmounting it, (ii) a transition layer in which the equations of motion proper apply. We take

[4] And the opposite will hold for the hours of the land breeze. We thus infer that islands can be expected to develop a strong turbulent diffusion by day and the reverse by night.

[5] This statement is based on the anticipation that the horizontal convergence must intensify (i.e., $\partial u/\partial r$ becomes increasingly negative) as we approach (i.e., as r increases) the front from its forward side.

[6] The results of our present study suggest that the treatment of a "moist" circulation is very desirable. See the closing sentence of Section 6.

that the thickness of the former is 25 m which enables us to obtain flow, temperature and pressure data for lower heights than was the case in our studies for a straight coast. As before, we assume that the combined depth of the two layers is 2 km.

b. Equations of the constant-flux layer: $0 \leqslant z \leqslant h$, $h = 25$ m

Assuming that the eddy viscosity equals the eddy conductivity, we have

$$\frac{\partial}{\partial z}\left(K\frac{\partial U}{\partial z}\right)=0, \quad U=(u^2+v^2)^{\frac{1}{2}}, \tag{4}$$

$$\frac{\partial}{\partial z}\left(K\frac{\partial \theta_T}{\partial z}\right)=0, \tag{5}$$

where

$$\text{(A)} \quad K=\lambda z^2\left(\frac{g}{\bar{\theta}}\left|\frac{\partial \theta_T}{\partial z}\right|\right)^{\frac{1}{2}}, \quad \text{for Ri} < -0.03, \tag{6a}$$

$$\text{(B)} \quad K=[k_0(z+z_0)(1+\alpha \text{Ri})]^2\frac{\partial U}{\partial z}, \quad \text{for } |1/\alpha| > \text{Ri} \gtrsim -0.03, \tag{6b}$$

$$\text{(C)} \quad K=2\times 10^4 \text{ cm}^2 \text{ sec}^{-1}, \quad \text{for Ri} \gtrsim |1/\alpha|. \tag{6c}$$

We have adopted the following values: $\lambda = 1$[7], $z_0 = 2$ cm for the island and $z_0 = 0.1$ cm for the sea, the latter allowing for a small measure of roughness of the sea surface. As to α, it was pointed out in Section 2 (end of second paragraph) that we were forced to assign to it the value -0.03, or a value close to -0.03, and a physical interpretation of the phenomenon was given in Section 2a.

c. Equations of the transition layer: $h \leqslant z \leqslant H$, $H = 2$ km

We place the origin of a cylindrical coordinate system at the center of our circular island. Since we assume an axisymmetric flow, all derivatives with respect to the azimuthal angle about the z axis vanish. Under such conditions and, using the symbol M for the magnitude of the relative angular momentum, the equations of motion, continuity, heat conduction, etc., are as follows:

$$\frac{\partial u}{\partial t}=-u\frac{\partial u}{\partial r}-w\frac{\partial u}{\partial z}+\frac{M}{r}\left(f+\frac{M}{r^2}\right)-\frac{1}{\rho}\frac{\partial p}{\partial r}+\frac{\partial}{\partial z}\left(K\frac{\partial u}{\partial z}\right) \tag{7}$$

$$\frac{\partial M}{\partial t}=-u\frac{\partial M}{\partial r}-w\frac{\partial M}{\partial z}-fru+\frac{\partial}{\partial z}\left(K\frac{\partial M}{\partial z}\right) \tag{8}$$

$$\frac{\partial w}{\partial t}=-u\frac{\partial w}{\partial r}-w\frac{\partial w}{\partial z}-\frac{1}{\rho}\frac{\partial p}{\partial z}-g \tag{9}$$

$$\frac{\partial \theta}{\partial t}=-u\frac{\partial \theta}{\partial r}-w\frac{\partial \theta}{\partial z}+\frac{\partial}{\partial z}\left(K\frac{\partial \theta}{\partial z}\right) \tag{10}$$

$$\frac{\partial w}{\partial z}=-\frac{1}{r}\frac{\partial (ru)}{\partial r} \tag{11}$$

$$M=rv, \quad p=\rho R_0 T, \quad \theta=T\left(\frac{p_0}{p}\right)^{R_0/C_p} \tag{12}$$

$$K=K(h)\frac{H-z}{H-h}. \tag{13}$$

d. Initial conditions, $t = 0$

$$p_1(z=0)=1000 \text{ mb} \tag{14}$$

$$T_1(z=0)\equiv\theta_1(z=0)=27\text{C} \tag{15}$$

$$T_1(z)=27-6.5\times 10^{-5}z \ (z \text{ in cm}). \tag{16}$$

e. Boundary conditions, $t \geqslant 0$

Before listing the boundary conditions, we wish to point out that the form adopted for the diurnal temperature wave at the land surface has been influenced by Kuo's (1968, Fig. 6) paper which is based on a radiative-convective model. The present form [given in Eq. (19)] is somewhat different from that which we used earlier [Neumann and Mahrer, 1971, Eq. (15c)] and was adopted in numerical experimentation subsequent to our 1971 paper. As before we let the amplitude of the first harmonic increase inland to a distance of 20 km from the coast. Beyond 20 km this amplitude is taken to be constant at its value at 20 km. The background of this decision is described on p. 535 of our 1971 study.

[7] The parameter λ is a nondimensional constant, identical with the ratio denoted H^* by Priestley (1959, p. 41). He suggested (p. 44) that the value of H^* is about 0.9. Some Russian investigators thought (Webb, 1965, p. 34) that the appropriate value is 0.8, while Webb (p. 36), who denotes the constant by the symbol h, puts $h = 0.94$. Dyer (1967, p. 505) finds, from an analysis of micrometeorological data for Kerang and Hay, Australia, that the "best" value for H^* is 1.15 ± 0.07. On rewriting (7.37) in the recent text by Monin and Yaglom (1971) and following their discussion on pp. 435–446, one comes to the conclusion that, implicitly, these authors favor the value of about 0.9. Because of the uncertainties involved, we have thought it wise to adopt at this stage the value 1 for $\lambda \equiv H^* \equiv h$. Further, we note that the form of K in (6a) is the form appropriate to the range of validity of Priestley's $-\frac{4}{3}$ law for the temperature and wind gradients in the constant-flux layer in very unstable air. For a more recent discussion of the temperature and wind profiles in conditions of static instability, and, especially, at high instability, see, e.g., Businger *et al.* (1971), Tennekes (1970) and Wyngaard *et al.* (1971).

TABLE 1. Data for the two model islands and for the numerical calculation.

	Radius R (km)	Distance from coast of lateral boundary out to sea L (km)	Horizontal grid Δr (km)	Vertical grid Δz (m)	Time step of integration $\Delta t \approx \frac{(\Delta z)^2}{K}$ (sec)	Geographical latitude φ (N)
Large island	$51.25=50+\frac{1}{2}\Delta r$	58.75	2.5	100	25	30
Small island	$26.25=25+\frac{1}{2}\Delta r$	28.75	2.5	100	25	30

The boundary conditions are as follows.

$$z=0: \quad u=v=w=0 \tag{17}$$

$$T_T(r>R)\equiv T_1(r>R)=27\text{C}, \quad T(r>R)\equiv 0 \tag{18}$$

$$T_T(R>r\gtrsim 20 \text{ km}, t) = 27+\left(12+\frac{x}{10}\right)\sin(15t-110) +3.5\sin(30t+75)+0.5(45t+66) \tag{19}$$

$$T_T(r<20 \text{ km}, t)\equiv T_T(r=20 \text{ km}, t) \tag{20}$$

$$T_T(r=R,t) = \tfrac{1}{2}[T_T(r=R-\Delta r, t)+T(r>R,t)]. \tag{21}$$

In (19) x is the distance (km) from the coast and t is in hours with $t=0$ at midnight.

$$z=H: \quad u=v=w=\theta=p^*=0 \tag{22}$$

$$r=0: \quad u=v=0 \tag{23}$$

$$r=R+L: \quad w=p^*=0, \quad \frac{\partial}{\partial r}(u,M,\theta)=0. \tag{24}$$

Since we are using a *staggered* grid (see Section 4), this explains why w and p are not specified for $r=0$.

4. Numerical aspects

As in our previous studies, we follow a procedure proposed by Chorin (1968) which we have extended to include the Coriolis terms. As in our SBF study (Neumann and Mahrer, 1973), we apply Liebmann's "accelerated" method to obtain the pressure by iteration from a Poisson-type equation. The essential steps of the numerical procedure are described in brief in Appendix B.

We use a staggered grid with

u,v computed at

$$r=(i-1)\Delta r, i=1,\ldots,\left(\frac{R+L}{\Delta r}+1\right), \tag{25}$$

w,p,T,θ computed at

$$r=(i-\tfrac{1}{2})\Delta r, i=1,\ldots,\frac{R+L}{\Delta r}. \tag{26}$$

As a consequence of (25) and (26) boundary conditions at the island center had to be imposed on u and v only. The radial distance L, counted from the coast to the seaward boundary of the integration, was so chosen that $R+L$ is an integral multiple of Δr.

Our studies have been carried out with respect to two model islands as set out in Table 1.

In order to remove the possibility of a nonlinear instability, we follow a smoothing procedure proposed by Shuman (1957). If ξ is the field (for instance, u, v) to be smoothed and S a smoothing element, then the smoothed value, $\tilde{\xi}$ say, of ξ is taken as

$$\tilde{\xi}_i=(1-S)\xi_i+S\frac{\xi_{i-1}+\xi_{i+1}}{2}. \tag{27}$$

We adopt $S=\frac{1}{2}$. Shapiro (1970, p. 362) points out that such a choice eliminates waves of length twice the grid interval. Waves shorter than two grid intervals, which are potentially dangerous to computational stability, are not amplified and even when they alias, they are damped. Longer waves are damped but not the very long ones. With $S=\frac{1}{2}$, our smoothing formula is

$$\tilde{\xi}_i=\tfrac{1}{2}\xi_i+\frac{\xi_{i-1}+\xi_{i+1}}{4}. \tag{27a}$$

It will be noted that (7) and (8) do not include terms representing horizontal diffusion. They were omitted in view of the fact that the smoothing procedure (27) amounts to a powerful diffusion process. In order to assess the degree of smoothing involved in (27a), we conducted some experiments. In these we have dropped, temporarily, the smoothing by (27a) but, instead, have formally added to the equations of motion, both for the straight coastline and for the circular islands, horizontal diffusion terms with a constant horizontal diffusion coefficient K_H. In the case of the first, a $K_H=2.5\times10^8$ cm^2 sec^{-1} was sufficient to prevent nonlinear instability (total length of period of integration 72 hr). In the case of the islands, not even a value of $K_H=5\times10^8$ cm^2 sec^{-1} was enough to forestall instability which set in after a time equivalent to 2 hr. Obviously, the effect of (27a) is much greater than that of a horizontal diffusion coefficient of the stated magnitude.

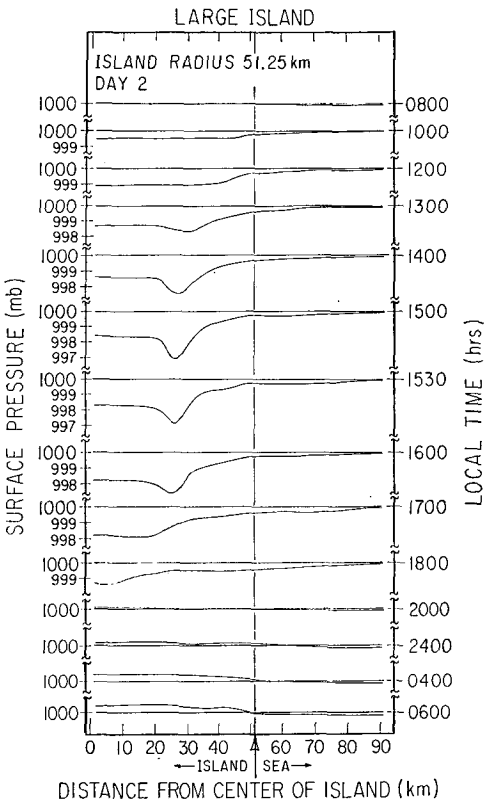

FIG. 1. Surface pressure as a function of time of day (Day 2 of integration) and of distance from the center of the large island.

5. Results

Of the two island SLBC's studied, that of the large island is the more interesting dynamically. We will discuss it first along with the presentation of a number of diagrams based on the second day of integration. We may add, though, that there is little difference between the results for the second and the third days. It is worth stressing that in Figs. 2–7 and 9–11 the arrows represent the horizontal wind. For instance, an arrow parallel with the abscissa which is directed to the left depicts a wind blowing toward the center of the island.

a. Large Island

1) PRESSURE

Perhaps the most striking, and to date the least appreciated, feature of the SLBC is the rapid development of a low-pressure system, albeit that of a shallow warm low. While at 1200 (all times local) the pressure over the island surface is very nearly *uniformly* low (Fig. 1), early in the afternoon a center of low pressure develops due to the dynamic instability of the SBF. As the front penetrates inland, the low deepens, the lowest pressure being reached about 1500 midway between the coast and the center when and where the pressure is 3.1 mb lower than over the sea. Many of the features described below, such as the growth of strong convergence/divergence fields, increasing vertical velocities, and warping of the isothermal surfaces are connected with this low. Just ahead of the front, the isothermal surfaces curve strongly upward up to an altitude of about 1700 m [Figs. 3 and 4; note the changes from 1000 (Fig. 2) to 1230 (Fig. 3)] but above that altitude there are indications of a downward warping which probably means that at these greater heights we are in a region of high pressure [see also Fig. 8 in Neumann and Mahrer (1973)]. The filling of the low is due to the fact that in the mid-afternoon the supply of energy through the upward transfer of heat falls off and it is no longer sufficient to feed the circulation.

2) THE SEA BREEZE IN THE LOWER AIR LAYERS

The strongest winds occur just behind the SBF and not on the coast as some traditional accounts would have it, except for the short period when the front is still close to the shore. The gradual strengthening of the just-behind-the-front breezes as the front progresses inland, is quite marked. Additionally, at the time of the greatest development of the surface low

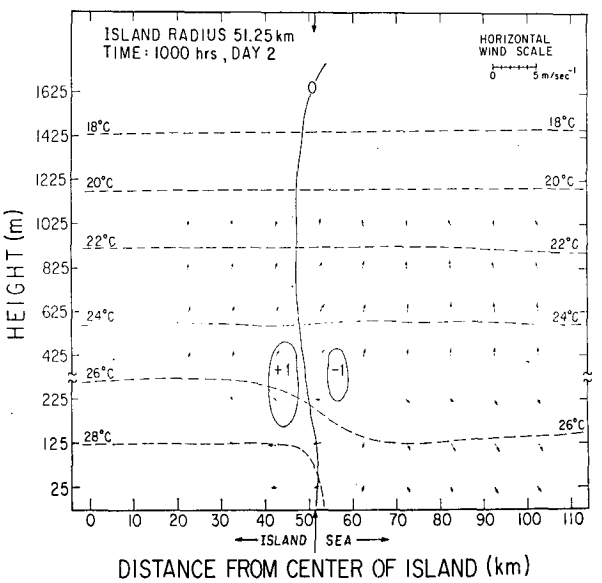

FIG. 2. Horizontal winds (arrows), vertical velocities (cm sec^{-1}, thin full lines) and temperatures (°C, thin dashed lines) for 1000 local time, Day 2, for the large island. The base points of the arrows are placed at the altitudes for which the arrows represent the horizontal wind. An arrow which is parallel with the abscissa and which is directed to the left symbolizes a horizontal wind that blows toward the center axis of the island. The winds are plotted for every fourth grid interval in the horizontal and for every other grid interval along the vertical. Length of arrow indicates wind speed (see scale at right-hand top corner of diagram). Note that the lower part of the ordinate does not have the same height scale as its upper part. Island radius of 51.25 km $=50$ km $+\frac{1}{2}\Delta r$, where $\Delta r=2.5$ km is the horizontal grid interval.

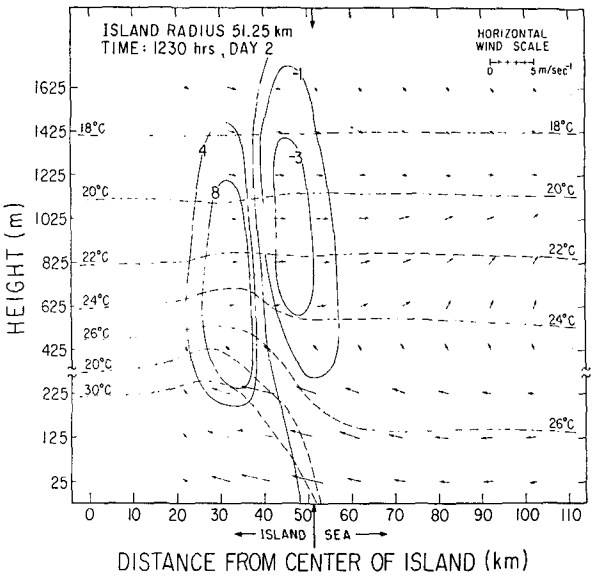

FIG. 3. As in Fig. 2 except for 1230 local time.

about the front, the winds *ahead* of the front are nearly opposite in direction to that of the sea breeze (a difference amounting to 120° to 150°, as shown in Figs. 4 and 5).

3) COUNTERCIRCULATION ALOFT

The conventional picture of a countercirculation aloft does not do full justice to the SLBC. According to our results, from about 1300 to about 1600 hours (see Figs. 4 and 5), the "upper" winds just ahead

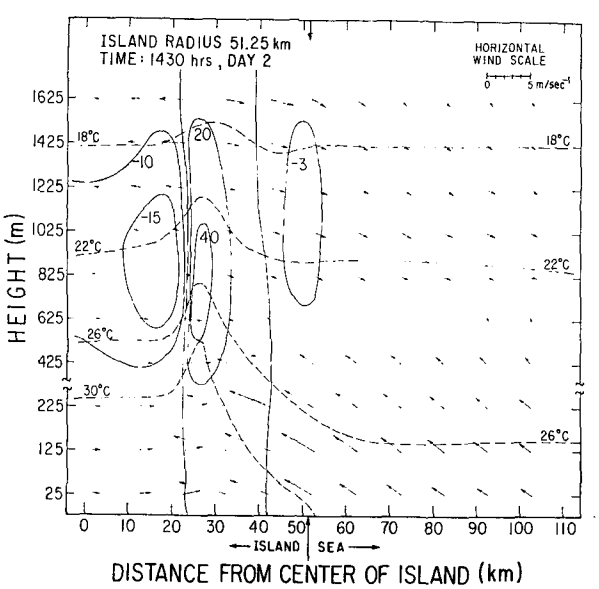

FIG. 4. As in Fig. 2 except for 1430 local time. Note formation of "eye" around island center, and low-level winds of nearly opposite directions astride the sea-breeze front which is situated at between 25 and 30 km.

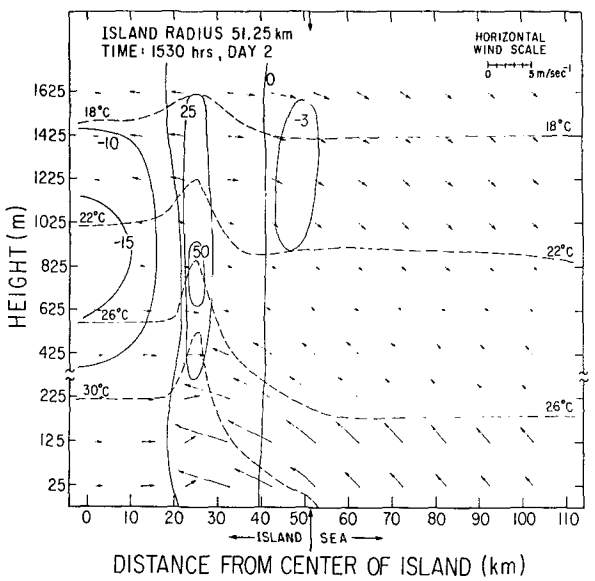

FIG. 5. As in Fig. 2 except for 1530 local time. Note low-level winds of nearly opposite directions astride the sea-breeze front which is situated nearly in the same position as in Fig. 4.

of the surface front blow more or less *in the same direction as the low-level sea breezes*. It is behind the front aloft that the winds comply with the idea of a countercirculation. Thus, above and just ahead of the front we have a strong horizontal divergence. An application of the integral

$$-g\int_0^H (\rho w)\left[\frac{1}{r}\frac{\partial(\rho u r)}{\partial r}+\frac{\partial(\rho\omega)}{\partial z}\right]dz,$$

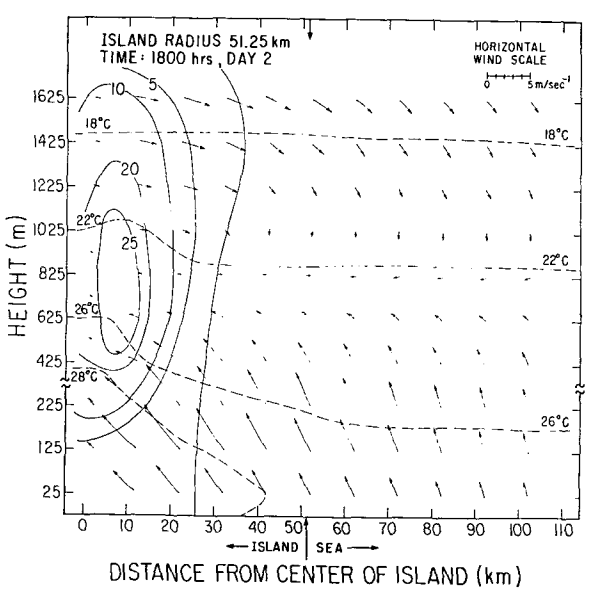

FIG. 6. As in Fig. 2 except for 1800 local time. Note that the "eye" has disappeared. The island center now is a region of upward motion.

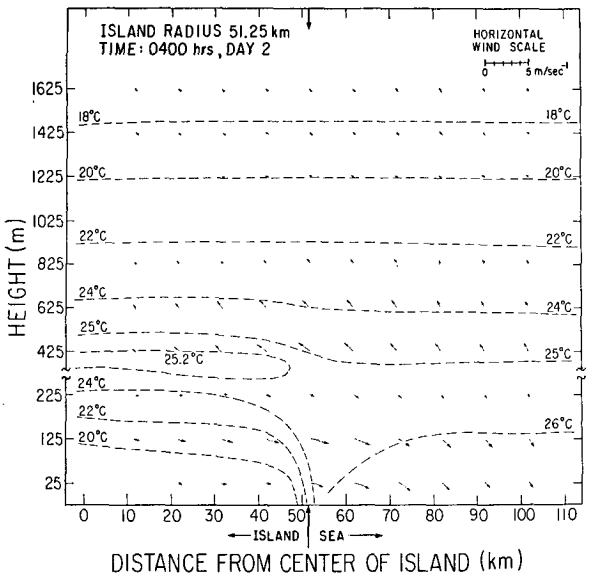

FIG. 7. As in Fig. 2 except for 0400 local time showing the land breezes. Note that the largest velocities occur out at sea. The land breezes are horizontally divergent. This diagram is representative of all night hours as changes during the night are minor.

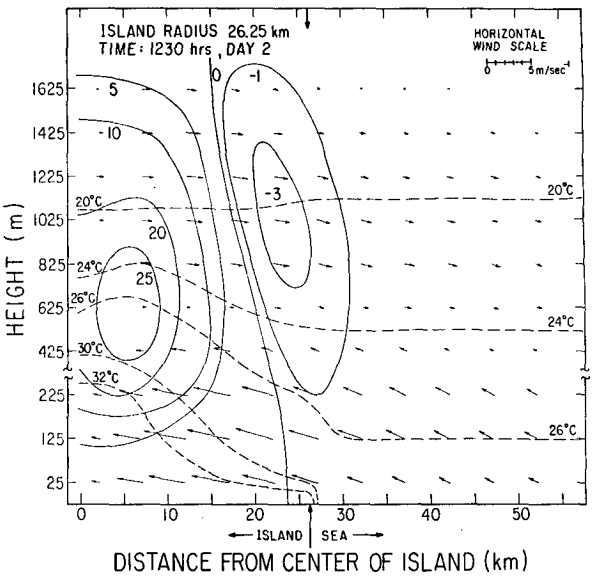

FIG. 9. As in Fig. 2 but for the small island at 1230 local time. Island radius of 26.25 km = 25 km + $\frac{1}{2}\Delta r$, where $\Delta r = 2.5$ km is the horizontal grid interval.

indicates that it is mainly this upper level divergence which is responsible for the pressure drop at and near the surface.

4) HORIZONTAL CONVERGENCE/DIVERGENCE

Some mention of this field was made in the foregoing paragraph. At low levels, up to 400–500 m, there is a strong convergence of the winds ahead of the front, and a horizontal divergence in the rear of it (see Figs. 3–5). The reverse distribution occurs aloft.

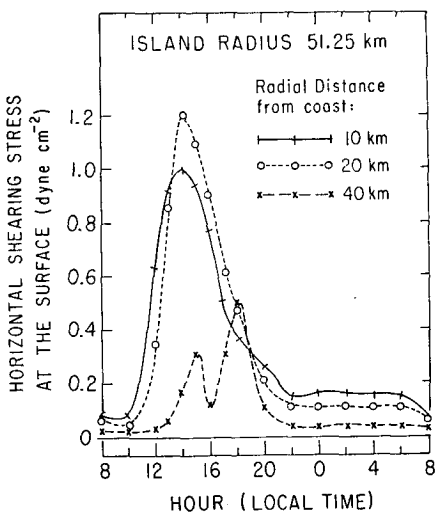

FIG. 8. Horizontal turbulent shearing stress at three positions as function of time of day for Day 2 on the large island. Note increase of shearing stress at point 40 km from coast about 1800 local time. It is close to this time that the sea-breeze front passes the position of concern.

5) VERTICAL VELOCITIES

A notable feature of the SLBC is the development of a cell of comparatively large upward velocities just above the front—up to about 50 cm sec^{-1} as shown in Fig. 5. It is almost certain that with a shorter horizontal grid interval (and a less powerful smoothing procedure) we would have found higher values of the vertical velocities.

The cell of downward velocities behind the front is rather underdeveloped compared with the one forming in the case of a straight coast (Neumann and Mahrer, 1973, Fig. 6) and it is nearly stationary just inland from the shore. The most surprising feature of our results, however, is the appearance and growth of a kind of an "eye" of downward velocities ahead of the SBF around the island center and subsequently at the center proper (Figs. 4 and 5). At 1800 in Fig. 6, there is no eye any longer at the center; the cell of upward velocities is now situated there.

6) TEMPERATURES

From about 1200 to 1600 (Figs. 3–6) the isothermal surfaces increasingly warp upward just ahead of the front. The greatest uplift occurs, of course, where we have the cell of upward motion. These surfaces display a steep drop seaward (cold air in rear of the front) and a gentle one toward the center. While the eye is warmer than the air behind the front, it is warmer than the air just ahead of it. Thus, the sea-breeze

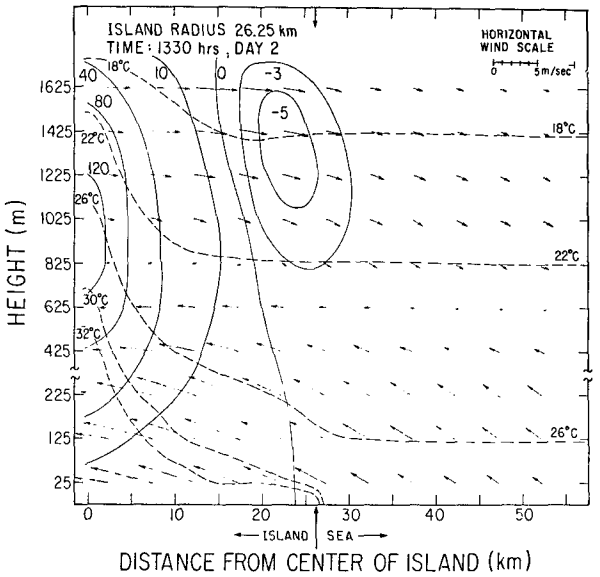

FIG. 10. As in Fig. 9 except for 1330 local time.

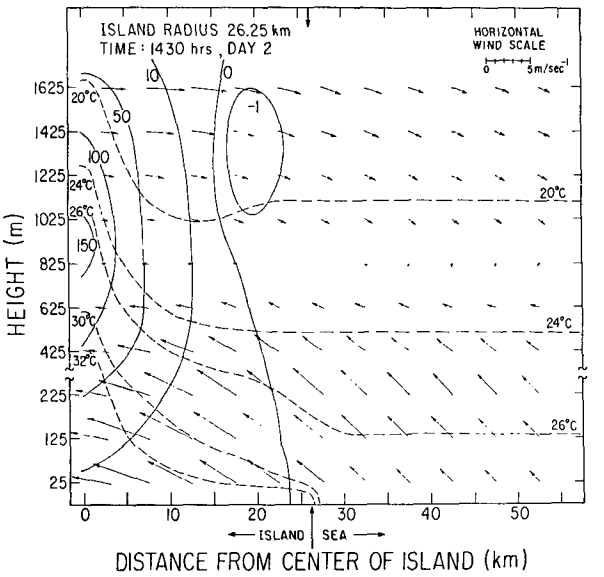

FIG. 11. As in Fig. 9 except for 1430 local time.

eye of islands has a structure different from that of hurricanes.

7) RATE OF ADVANCE OF SBF

While between 1000 and 1200, as well as between 1600 and 1700 hours, the speed of progression of the front is about 5 km hr^{-1}, and up to 10 km hr^{-1} between 1700 and 1800, the total advance from 1300 to 1600 is only about 5 km. The more intense the dynamic developments are along the front, the smaller is its rate of progression: the equation of continuity indicates that the high upward velocities are at the expense of the winds ahead of the front.

8) SHEARING STRESS IN THE CONSTANT-FLUX LAYER

One other striking result of the present study is offered by Fig. 8. At 40 km inland the shearing stress declines after 1500. The SBF at that time is about 14 km closer to the coast, and the winds are still weak. The decline in the shearing stress is probably due to the lessening static instability in the air. However, at about 1800 (Fig. 6) the front approaches the point radially 40 km from the coast, the winds pick up, and turbulence and shearing stress increase, despite the growing static stability in the air.

9) LAND BREEZES

The land breezes are weak as shown in Fig. 7, but they are stronger at sea than over the island. In fact, they are stronger out to sea than just offshore. This is in keeping with the expected (Neumann, 1951a, b) divergent character of the land breezes in regions of convex coastlines (convex toward the sea). We only present one diagram for the land breeze phase of the circulation due to the fact that the changes at night are minor.

b. Small island

Although the vertical velocities reached by SLBC of the small island are about three times greater

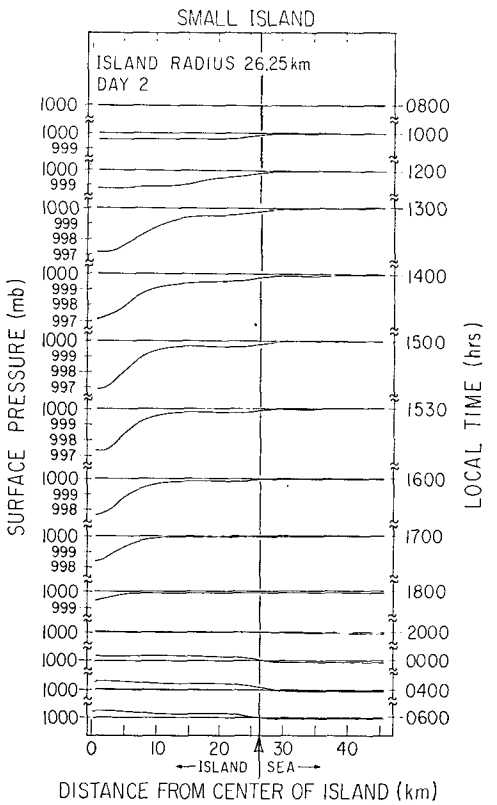

FIG. 12. As in Fig. 1 except for the small island.

(150 cm sec^{-1} at 1400 and 1430 as shown in Fig. 11) than is the case for the large island, the dynamic developments are far less diversified. Since the coastline to island center distance is small, the sea breeze reaches the center at the relatively early hour of 1300 (Figs. 9 and 10). Not enough heat can be supplied by the island surface to the air to feed the instability incipient about the front. Nowhere near the surface do we find that any significant difference between the direction of the winds ahead of the front and to those in its rear. Aloft we find a rather strong conventional countercirculation reaching to $\sim$1700 m (Fig. 11). The convergence/divergence fields are strongly developed and, at the time of the maximum upward velocity, the lowest surface pressure, at the center, is about 3.1 mb lower than out at sea (Fig. 12).

While in the case of the large island the circulation keeps intensifying until close to 1600 hours, in the case of the small island the circulation decays after about 1430. By 1800 the winds at sea are nearly tangential to the island. And, as is true for the large island, the changes during the night are small. Again, the winds out at sea are stronger than inland. Fig. 7 for the large island does not differ much from the figure appropriate to the small island at the same time. The nocturnal pressure distribution (Fig. 12) is rather flat, with pressure over the island being about 0.4 mb higher than out to sea. In closing we add that the flow situation at 1000 is rather similar to that of the large island shown in Fig. 2.

6. Concluding comments and summary

The most outstanding and so far little noted feature of the SLBC is the frontal instability and circulation features (such as a migratory intensifying pressure fall, marked horizontal convergence ahead and divergence in the rear of the front in the lower air layers, the reverse distribution aloft, strong warping of the isothermal surfaces, etc.) evolving along the SBF, resembling the processes taking place along synoptic-scale cold fronts. In the case of islands, and especially in the case of islands of a radius comparable with the "normal" linear dimensions of the SLBC for a given diurnal temperature wave, the developments are much more pronounced than in the case of a straight coastline. The greater intensity is due to the much stronger horizontal convergence of the sea breezes. One of the surprising results is the formation of a kind of an "eye" of downward motion at the island center (of the large island). The low-level sea breezes are horizontally convergent, especially in the vicinity of the SBF, whereas the land breezes are divergent.

The SLBC of the large island departs to some extent from the conventional picture of that circulation. Winds ahead of the SBF are, for some time, nearly opposite in direction to that of the sea breezes behind the front. Aloft, not all winds comply with the idea of a countercirculation: winds ahead of the front blow nearly in the same direction as the low-level sea breezes.

Some observations confirm several features of the pattern obtained in our calculations. Reference is made to a diagram of the SBF at Cape Cod (Wallington, 1961, Fig. 11.3). Though Cape Cod is a peninsula rather than an island, its shape is closer to that of islands than of any other land body for which at least some of the requisite observations are available. Additionally, we quote observations taken in southern England. Although the location cannot be considered an island location for the purposes on hand, nevertheless the observations have a strong bearing on our results. Thus, the nearly opposite directions of the winds astride the SBF when it is well developed are illustrated by Simpson's data (1964, p. 211) while vertical velocities of 1–6 m sec^{-1} are reported by Mackenzie (1956, p. 295), Wallington (1961, Fig. 11.4; the data are partly due to Mackenzie) and Simpson (1965, p. 654).

Despite the above-mentioned observational reports, which agree in a qualitative and, perhaps, a semi-quantitative manner with our predictions, it is clear that our results (as are the results of all studies involving modelling of the not-too-well-understood processes of turbulence, integrations of nonlinear differential equations, and smoothing procedures) are subject to uncertainties. However, the comments advanced in the next paragraph seem to be well-founded.

It has been customary to assume that the most important features of the sea breeze are found near the coast. The opposite seems to be true. The most interesting developments, including the largest velocities, form a few tens of kilometers inland. Conversely, the most marked characteristic of the otherwise feature-poor land breeze, namely, its speed, is greater out at sea at a distance from the coast, rather than close to it. The large upward velocities developing in the case of island SLBC's suggest that it would be worthwhile to study models making allowance for the formation of clouds.

Acknowledgments. The writers are pleased to record their indebtedness to The Department of the Geophysical Sciences (Prof. George W. Platzman, Chairman), of The University of Chicago, for providing the secretarial and technical assistance needed for the preparation of the manuscript for publication; Mrs. Marilyn Hinds typed the manuscript. The numerical calculations were carried out on the Hebrew University's CDC 6400 computer in Jerusalem.

APPENDIX A

List of Symbols

C_p	specific heat at constant pressure
f	Coriolis parameter

g acceleration of gravity
h thickness (25 m) of constant-flux layer
H height (2 km) of layer affected by the SLBC
k_0 von Kármán's constant
K (vertical) eddy viscosity or conductivity
K_H horizontal eddy viscosity
L radial distance from coast of boundary of SLBC out at sea
M relative angular momentum $[=rv]$
p pressure; p_0 reference pressure
p^* deviation of pressure from its instantaneous hydrostatic value p_H $[p_T=p_H+p^*]$
r radial distance
R radius of island
R_0 gas constant
Ri Richardson number
t time
u_i, or u, v, w radial, tangential and vertical components of velocity $(i=1, 2, 3)$
$\bar{u}_i$, or $\bar{u}, \bar{v}, \bar{w}$ same as u_i, or u, v, w except that the latter are now considered as components of the mean wind in turbulent flow
u_i', or u', v', w' turbulent components of flow
U $[=(u^2+v^2)^{\frac{1}{2}}]$
x_i, or x, y, z Cartesian coordinates, x directed along r [in (19) x is the distance from the coast toward the island center]
z_0 roughness parameter
α nondimensional constant [see (6b)]; $(-1/\alpha)$ is, roughly speaking, a critical Richardson number
θ potential temperature; $\tilde{\theta}$, average potential temperature for a layer
λ nondimensional constant [see (6a)]
ρ density $[\equiv\rho_T]$
φ geographical latitude

p, T and θ without the subscripts 1 or T denote disturbance variables—subscript 1 symbolizes initial, undisturbed, value; subscript T [=total] denotes sum of initial and disturbed value, e.g., $p_T=p_1+p$.

APPENDIX B

The Finite-Difference Scheme for the Retrieval of Pressure

It is pointed out in Section 4 that the numerical method which we adopted was influenced by Chorin's (1968) paper. As far as we know, the method we followed has not been used in meteorology. (The foregoing statement applies up to the point where the Liebmann "accelerated" iteration procedure is introduced.) For that reason, we will describe here, as briefly as possible, the most difficult stage of the calculation, namely, the solution of a Poisson-type equation for the pressure.

Let I be the serial number of the grid points in the horizontal, $I=1,\cdots,\{[(R+L)/\Delta r]+1\}=M$, say, and J the corresponding quantity along the vertical, $J=1,\cdots,N$, where $J=1$ represents $z=0$, $J=2$ the point $z=h$ (the top of the constant flux layer); Δt, Δr and Δx denote, respectively, the length of the time step, horizontal (radial) and vertical grid intervals. Following Chorin (1968), the calculation of u and w is split into two steps. First, we omit the pressure gradient terms and compute the velocities u^* and w^*; next, we re-introduce the pressure gradient terms to compute u and w. Thus, we write

$$p_T=p^*+p_H, \tag{B1}$$

p^* being the deviation of pressure from the instantaneous hydrostatic value p_H; we calculate p_H

$$\frac{\partial p_H}{\partial z}=g\left(\frac{p_1}{R_0T_1}-\frac{p_T}{R_0T_T}\right). \tag{B2}$$

Assuming, for simplicity's sake, that

$$\rho(I,J)=\rho(I-1,J)=\rho(I,J+1)=\rho(I,J-1), \tag{B3}$$

our equations for u, u^*, etc., will be as follows (u, u^*, w, w^*, ρ and p^* all relate to the same time step):

$$u(I,J)=u^*(I,J)-\frac{\Delta t}{\rho(I,J)}\frac{p^*(I+1,J)-p^*(I,J)}{\Delta x} \tag{B4}$$

$$u(I-1,J)=u^*(I-1,J)-\frac{\Delta t}{\rho(I,J)}\frac{p^*(I,J)-p^*(I-1,J)}{\Delta x} \tag{B5}$$

$$w(I,J+1)=w^*(I,J+1)-\frac{\Delta t}{\rho(I,J)}\frac{p^*(I,J+2)-p^*(I,J)}{2\Delta z} \tag{B6}$$

$$w(I,J-1)=w^*(I,J-1)-\frac{\Delta t}{\rho(I,J)}\frac{p^*(I,J)-p^*(I,J-2)}{2\Delta z}. \tag{B7}$$

In terms of finite differences the equation of continuity (11) takes the form

$$\frac{r(I)u(I,J)-r(I-1)u(I-1,J)}{r(I-1/2)\Delta r}+\frac{w(I,J+1)-w(I,J-1)}{2\Delta z}=0, \tag{B8}$$

where

$$r(I-\tfrac{1}{2})=\tfrac{1}{2}[r(I)+r(I-1)].$$

We multiply (B4) by $r(I)/[r(I-\frac{1}{2})\Delta r]$, (B5) by $r(I-1)/[r(I-\frac{1}{2})\Delta r]$, and (B6) and (B7) by $1/(2\Delta z)$. We can then combine (B4)–(B8) to yield one equation. After multiplying the combined equation by $4\Delta z^2\rho(I,J)/\Delta t$ and writing, for short,

$$F_{I,J}(u^*,w^*)=\frac{4\Delta z^2\rho(I,J)}{\Delta t}\times\left[\frac{r(I)u^*(I,J)-r(I-1)u^*(I-1,J)}{r(I-1/2)\Delta r}+\frac{w^*(I,J+1)-w^*(I,J-1)}{2\Delta z}\right], \quad \text{(B9)}$$

$$S=\frac{4\Delta z^2}{\Delta r^2}, \quad \text{(B10)}$$

we find that

$$p^*(I,J+2)+p^*(I,J-2)-2(1+S)p^*(I,J)+S\left[\frac{r(I)}{r(I-1/2)}p^*(I+1,J)+\frac{r(I-1)}{r(I-1/2)}p^*(I-1,1)\right]-F_{I,J}(u^*,w^*)\begin{cases}=0, & \text{ideally}\\ =D, & \text{say, with } D\neq 0 \text{ often in practice}\end{cases} \quad \text{(B11)}$$

From now on the procedure is "standard." We adopt a value ϵ and prescribe that D must be numerically less than ϵ (we have chosen $\epsilon=10^{-7}$). If D is not less than ϵ, we apply the Liebmann accelerated iteration process in the form

$$p^{*m+1}=p^{*m}+\frac{(1+\alpha)D}{2(1+S)}, \quad \text{(B12)}$$

α being the "over-relaxation" coefficient; it is determined [Miyakoda, 1960 (4.11)] in terms of the number of grid points by the equation

$$\alpha=1-\left\{2\left[\left(\frac{\pi}{M-1}\right)^2+\left(\frac{\pi}{N-1}\right)^2\right]\right\}^{\frac{1}{2}}. \quad \text{(B13)}$$

In the case of our large island, we have adopted $M=44$, $N=21$, leading to $\alpha=0.75$; in the case of the small island, $M=22$, $N=21$, or $\alpha=0.69$. We have worked with the value $\alpha=0.70$.

Generalizing Miyakoda's (1960) Eq. (4.1), we reach the final form of the iteration equation as follows:

$$p^{*m+1}(I,J)=p^{*m}(I,J)+\frac{1+\alpha}{2(1+S)}\left[p^{*m}(I,J+2)+p^{*m+1}(I,J-2)-2(1+S)p^{*m}(I,J)+\frac{r(I)}{r(I-1/2)}Sp^{*m}(I+1,J)+\frac{r(I-1)}{r(I-1/2)}Sp^{*m+1}(I-1,J)-F_{I,J}(u^*,w^*)\right]. \quad \text{(B14)}$$

As long as $I=3,\cdots,(M-1)$, and $J=4,\cdots,(N-2)$, no boundary grid points are involved in (B14). We will now consider two cases where boundary conditions will enter.

a. The case $I=2$

If $I=2$, then $I-1=1$, the latter representing grid points along the vertical axis at the island center, this axis being a boundary. By dint of (23), $u(1,J)=0$ and this will affect some terms in (B5) and (B8). In any case, in the latter $r(1)=0$. With $u(1,J)=0$ we anticipate that $u^*(1,J)=0$ and $p^*(I,J)=0$ as well as $p^*(2,J)=0$ very nearly. Thus we are left with (B4) and (B6)–(B8). Repeating the procedure that has led to (B14) and noting that $[r(2)/r(1.5)]=2$, we reach the result that

$$p^{*m+1}(2,J)=p^{*m}(2,J)+\frac{1+\alpha}{2(1+S)}\left[p^{*m}(2,J+2)+p^{*m+1}(2,J-2)+2Sp^{*m}(3,J)-2(1+S)p^{*m}(2,J)-F_{2,J}(u^*,w^*)\right]. \quad \text{(B15)}$$

b. The case $J=3$

This case represents the grid points at height $z=h+\Delta z$. As long as Δr is large relative to Δz, we can expect the solution for pressure to be very close to hydrostatic, especially near the surface. If then in (B7) we put $p^*(I,3)=p^*(I,1)=0$, we find that $w(I,2)=w^*(I,2)$ to a close approximation. Repeating the procedure which has led to (B14), it is found that

$$p^{*m+1}(I,3)=p^{*m}(I,3)+\frac{1+\alpha}{1+2S}\left\{p^{*m}(I,5)+S\left[\frac{r(I)}{r(I-1/2)}p^{*m}(I+1,3)+\frac{r(I-1)}{r(I-1/2)}p^{*m+1}(I-1,3)\right]-(1+2S)p^{*m}(I,3)-F_{I,3}(u^*,w^*)\right\}. \quad \text{(B16)}$$

We have carried out numerical experiments. These indicate that what is said above for the case $J=3$ is *very* closely satisfied in all grid intervals except the one where the sea-breeze front is located. However, even for that interval the approximation is close. Naturally, if the ratio $\Delta r/\Delta z$ is small, or if a nested grid is used in order to be able to get detailed information for the frontal region, one would have to revert to (B14).

Finally, it should be pointed out that the boundary condition $p^*=0$ at $z=H$ [see (22)] is not a necessity. Rather, it facilitates the computation. For, if the pressure is kept constant at $z=h$, one can then conveniently calculate the pressure at any lower altitude by integrating from $z=H$ downward. Also, the convergence of the iteration process increases rapidly by the condition $p^*=0$.

REFERENCES

Businger, J. A., J. C. Wyngaard, Y. Izumi and E. F. Bradley, 1971: Flux-profile relationships in the atmospheric surface layer. *J. Atmos. Sci.*, **28**, 181–189.

Byers, H. R., and H. R. Rodebush, 1948: Causes of thunderstorms of the Florida peninsula. *J. Meteor.*, **5**, 275–280.

Chorin, A., 1968: Numerical solution of the Navier-Stokes equations. *Math. Comput.*, **22**, 745–762.

Dyer, A. J., 1967: The turbulent transport of heat and water vapour in an unstable atmosphere. *Quart. J. Roy. Meteor. Soc.*, **93**, 501–508.

Ellison, T. H., 1957: Turbulent transport of heat and momentum from an infinite rough plane. *J. Fluid Mech.*, **2**, 456–466.

Estoque, M. A., 1961: A theoretical investigation of the sea breeze. *Quart. J. Roy. Meteor. Soc.*, **87**, 136–146.

——, 1962: The sea breeze as a function of the prevailing synoptic situation. *J. Atmos. Sci.*, **19**, 244–250.

Kuo, H. L., 1968: The thermal interaction between the atmosphere and the earth and propagation of diurnal temperature waves. *J. Atmos. Sci.*, **25**, 682–706.

Lumley, J. L., and H. A. Panofsky, 1964: *The Structure of Atmospheric Turbulence*. New York, Interscience, 239 pp.

Mackenzie, J. K., 1956: Exploring the sea-breeze front. *Sailplane Gliding*, **7**, 294–296.

McPherson, R. D., 1970: A numerical study of the effect of a coastal irregularity on the sea breeze. *J. Appl. Meteor.*, **9**, 767–777.

Miyakoda, K., 1960: Test of convergence speed of iterative methods for solving 2 and 3 dimensional elliptic type differential equations. *J. Meteor. Soc. Japan*, **38**, 107–124.

Monin, A. S., and A. M. Yaglom, 1971: *Statistical Fluid Mechanics: Mechanics of Turbulence*, Vol. 1. The MIT Press, 769 pp.

Neumann, J., 1951a: Land breezes and nocturnal thunderstorms. *J. Meteor.*, **8**, 60–67.

——, 1951b: Diurnal variation of low cloudiness in summer at two stations situated near coastlines of opposite curvature. Meteor. Notes, Ser. A, No. 2, Israel Meteorological Service, 14 pp.

——, 1973: Flows with both vertical and horizontal shears and the critical Richardson number. Submitted for publication.

——, and Y. Mahrer, 1971: A theoretical study of the land and sea breeze circulation. *J. Atmos. Sci.*, **28**, 532–542.

——, and ——, 1973: Evolution of a sea breeze front: A numerical study. *Climatological Research, The Hermann Flohn 60th Birthday Volume*, Meteorological Institute, University of Bonn, 481–492.

Obukhov, A. M., 1971: Turbulence in an atmosphere with a non-uniform temperature. *Bound. Layer Meteor.*, **2**, 7–29. (Translation from the Russian original published in 1946 in *Tr. Akad. Nauk SSSR Inst. Teoret. Geofiz.*, No. 1, 95–115.)

Pielke, R., 1972: Comparison of a hydrostatic and an anelastic dry shallow primitive equation model. NOAA Tech. Memo. ERL OD-13, Boulder, Colo., 47 pp.

Priestley, C. H. B., 1959: *Turbulent Transfer in the Lower Atmosphere*. The University of Chicago Press, 130 pp.

Rosenthal, S. L., 1970: Experiments with a numerical model of tropical cyclone development. *Mon. Wea. Rev.*, **98**, 106–120.

Shapiro, R., 1970: Smoothing, filtering, and boundary effects. *Rev. Geophys. Space Sci.*, **8**, 359–387.

Shuman, F. G., 1957: Numerical methods in weather prediction: II. Smoothing and filtering. *Mon. Wea. Rev.*, **85**, 357–361.

Simpson, J. E., 1964: Sea-breeze fronts in Hampshire. *Weather*, **19**, 208–220.

——, 1965: The sea-breeze at Lasham. *Aero-revue*, **40**, 653–655.

Tennekes, H., 1970: Free convection in the turbulent Ekman layer of the atmosphere. *J. Atmos. Sci.*, **27**, 1027–1034.

Wallington, C. E., 1961: *Meteorology for Glider Pilots*. London, Murray, 284 pp.

Webb, E. K., 1965: Aerial microclimate. *Meteor. Monogr.*, **6**, No. 28, 27–58.

Wyngaard, J. C., O. R. Coté and Y. Izumi, 1971: Local free convection, similarity, and the budgets of shear stress and heat flux. *J. Atmos. Sci.*, **28**, 1171–1182.